IEIE Transactions on Smart Processing and Computing, vol. 10, no. 5, October 2021
https://doi.org/10.5573/IEIESPC.2021.10.5.398

Digital Radiography with a Consumer Camera: Image Denoising and Deblurring

Van-Giang Nguyen

Department of Information Systems, Le Quy Don Technical University, Hanoi, Vietnam giangnv@mta.edu.vn

Received April 22, 2021; Revised June 16, 2021; Accepted August 20, 2021; Published October 30, 2021

** Regular Paper*

***Abstract*:** Projection radiography is the most popular medical imaging modality due to its simple design and ease of use. To maintain quality, direct flat-panel detectors must be used to collect patient images, thereby providing a digital radiography (DR) imaging system. In this paper, we investigate an imaging system utilizing a DSLR camera to capture images from a scintillator illuminated by X-rays passing through the object to be imaged. However, maintaining the quality of the image from the proposed system is difficult since it contains impulsive-style noise, and blur varies based on distance. To get rid of unwanted radiographic impulsive noise, we use a statistical-based impulsive noise removal method. To handle the blurring issue in our proposed imaging system, we first use a systematic method to estimate the X-ray source and detector point spread functions (PSFs) from the radiographic image. The PSFs are then used in a non-blind deconvolution algorithm to deblur the image. Experiments on a variety of DR images show that with the proposed denoising and deblurring approaches, our imaging system can provide DR images with fine detail, and it can potentially be used for basic radiography.

***Keywords*:** X-ray imaging, Digital radiography, Deblurring, Denoising, Detector blur, Deconvolution

1. Introduction

Digital radiography (DR) is an X-ray radiographic imaging technology acquiring digital projection images using photo-stimulable storage phosphor (computed radiography, or CR), amorphous selenium, amorphous silicon, charge coupled devices (CCDs), or a metal-oxide semiconductor field effect transistor. Among many medical imaging modalities in digital radiography, the two most popular ones are computed radiography and flat-panel digital radiography [1].

In CR, a photo-stimulable phosphor is coated on the plate, referred to as an imaging plate (IP), which is housed in a cassette to protect it. The IP is then considered the digital detector in CR. However, this technology has some limitations. The spatial resolution is less than that from DR, and the total acquisition time and image reading time are much higher than DR. The durability of the IP is less than with a DR image.

Flat-panel digital radiography systems have been developed to overcome the shortcomings of CR systems. In DR, the digital detector is designed with a flat panel. Currently, there are two categories of flat-panel digital radiography imaging systems (based on the type of detector used [2]), and they have been popularly referred to as (i) indirect conversion digital radiography systems, and (ii) direct conversion digital radiography systems. The latter use detectors that convert X-rays directly to electronic signals, but in the former, X-rays are first converted into light using a phosphor. The emitted light from the phosphor falls upon a matrix array of electronic elements to create and store electrical charges in direct proportion to the X-ray exposure. The charges produce electrical signals that are subsequently digitized and processed by a computer to produce an image. These two types of modalities have high sensitivity but are expensive due to the involvement of a thin film transistor (TFT) array in the detector. In a second type of indirect conversion detector, charge coupled devices (CCDs) are coupled to a phosphor cesium iodide scintillator. X-rays hit the phosphor to produce light, which then hits the CCD array that converts the light into electrical signals, which are digitized and processed by a computer to produce an image.

While the above detector technologies result in superior DR image quality, the high price prevents use in rural areas and when imaging a large object. To reduce the price of the DR detector and increase its lifetime, attempts have been made to use a lens-coupled X-ray detector [3, 4]. That approach photographs a screen (usually an X-ray scintillator) exposed to X-rays. This collection of X-ray

photons can be done by coupling a scintillating screen and a camera, which captures the scintillating screen to create an X-ray image. However, since the optical sensors used in digital cameras are much smaller than the objects to be imaged, the camera must be moved far away from the illuminating scintillator so that the entire X-ray image fits on the sensor.

Inspired by that idea, in this paper, we built and investigated an imaging system that is likely to be cheaper than existing methods of X-ray imaging. Compared to the conventional indirect flat-panel system, the proposed imaging system uses a mirror to reflect the light from the scintillating screen to the camera. This mirror is used to prevent the incoming X-rays from hitting the camera sensor. This camera design is similar to the one used in high-resolution micro-CT [5], but not in digital radiography, as in this work.

On the one side, since the proposed imaging system shares some similarities with existing systems, the captured image has to go through an extensive image processing pipeline (described in Section 2) to produce the display image as closely as possible to currently used DR imaging techniques. One the other side, since the acquiring process is different from ordinary DR with existing flat-panel detectors, the acquired images are degraded by two factors: unwanted impulsive noise and blurring. The noise here is not only Poisson noise, but also *impulsive-style noise* that occurs during DSLR acquisition under dark conditions where the inner space containing the camera (including the mirror and the one side of the scintillator) has to be kept in total darkness to increase the sensitivity of the acquisition. The impulsive-style noise is caused by failures in sensors, readout circuits, A/D converters, or communication channels. This impulsive-style noise is not only found in our imaging system with a lens-coupled X-ray detector where the consumer camera takes the picture of the scintillating screen to create an X-ray image, but is also found in standard digital radiography, as reported in [6]. This impulsive-style noise, even at a low rate, leads to a poor visualization result (after the raw image goes through contrast enhancement). Furthermore, the acquired image in DR is also blurred due to source blur, detector blur, and motion blur. These two issues, especially the *impulsive-style noise*, were not addressed in previous work [3-5].

To address the noise issue, we use a statistical-based impulsive noise removal method and make it work in separate channels of the color image captured by the DSLR camera. This is to ensure that only impulsive-style noise is removed, while the detail is kept perfectly in the acquired image. To deblur the image, rather than using the blind deblurring method, which might result in an artificial image (with unwanted nonrealistic patterns), we use non-blind deblurring with a systematically derived blur kernel. Our deblurring framework consists of two steps: (i) estimating the X-ray source and detector point spread functions (PSFs) via the radiographs of a pre-designed metal plate, and (ii) using the estimated PSFs (the blur kernel) to perform deblurring via a non-blind deconvolution method. Our deblurring process takes into account the distance to the detector plane from the object to be imaged.

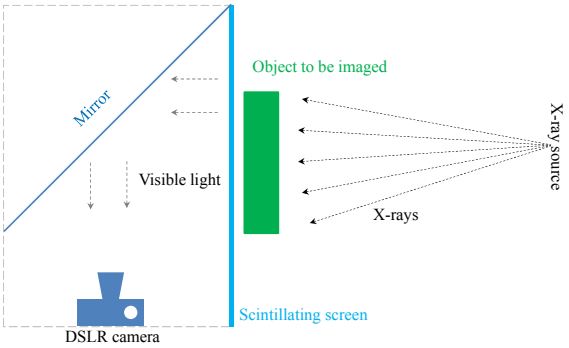

Fig. 1. Diagram of the proposed imaging system.

In Section 2, we describe the imaging system used to acquire the DR image, as well as the image processing pipeline to produce the final ready-to-display DR image. The section also describes a method to remove impulsive-style noise, and a method to deblur DR images. Section 3 presents results from using experimental data with our prototype DR imaging system. Section 4 concludes the paper.

2. Methods

2.1 Imaging Systems and Image Processing Pipelines

The working principle of the proposed imaging system is summarized in Fig. 1. It consists of an X-ray tube, a scintillating screen, a mirror, and a camera. When the X-rays are emitted, they come through the object being imaged. Some are attenuated by the object, and the remaining hit the scintillation screen. Depending on the number of X-rays that hit it, the scintillation screen will light up. At that moment, the camera opens its lens to capture an image of the scintillating screen. Note that, to protect the lens from being hit by X-rays passing through the scintillator, the camera takes an image of the mirrored scintillating screen. The captured image will be processed to generate a ready-to-display image.

To realize the idea, we built the prototype imaging system in Fig. 2. The system consists of the following main parts: (i) the X-ray source is a Toshiba Rotanode E7239X; (ii) the scintillator is a Hamamatsu GPXS J10666-100; and (iii) the consumer camera is a Canon EOS 750D. The X-ray source is synchronized with the camera so the camera will open its lens to acquire the light from the scintillating screen when it reaches its brightest state. The settings of the DSLR camera are as follows: shutter speed = 1/3 sec, ISO=800, and AV=10. The lens is locked in focus by taking an image of a resolution test chart placed behind the scintillating screen.

In digital radiography, regardless of the imaging system (the DR scanner), radiologists always want to view the image in the display device (for example, on an LCD monitor), and images (from different scanners) of the same patient should be the same. Therefore, we need to adopt an

Fig. 2. Our prototype DR with an indirect DSLR-based detector.

image processing pipeline to generate standardized, ready-to-display images. Regarding our proposed imaging system (with a DSLR-based detector), we use an image processing pipeline that consists of the following steps.

(i) Remove radiographic impulsive noise.

(ii) Use flat-field correction to correct the varying flat field in the image [7].

(iii) Image scaling determines the actual object region in the DR image.

(iv) Image deblurring (or edge restoration) handles blurring due to the detector and the X-ray source.

(v) Apply dynamic range reduction and latitude reduction [8].

(vi) Use multiscale contrast enhancement [9, 10]

The aim of image processing here is to eliminate all factors contributing to unwanted degradation in the acquired image, and to generate the final ready-to-display image (described in Section 3). Note that in our imaging system, steps (i) to (iv) are performed with a color image, while in steps (v) and (vi), the processing image is grayscale to match the standard in digital radiography.

Most factors that degrade the standard DR image quality (with an actual flat-panel detector) have been addressed in previous work [7-10]. However, regarding our DR imaging system with DSLR-based detector, there are two new degrading factors that have not been addressed in previous DR imaging systems. Those are impulsive-style noise, and blur in the image when capturing an object that is a little far from the scintillating screen.

2.2 Impulsive Noise Removal

In our imaging system, the acquired images are usually corrupted by impulsive noise, as shown in Figs. 3(a), 4(a) and 5(a). By analyzing the raw image (in our case, it is the CR2 file), which is a color sample output from an image sensor with a color filter array (CFA), we found that the noise shows up in the raw data (before demosaicing) and appears differently in different color filters and in nearby pixels. (See Figs. 3(b) to 3(e)). That eventually results in complex impulsive noise patches in the acquired RGB image in Fig. 3(a). We also found that the location of the

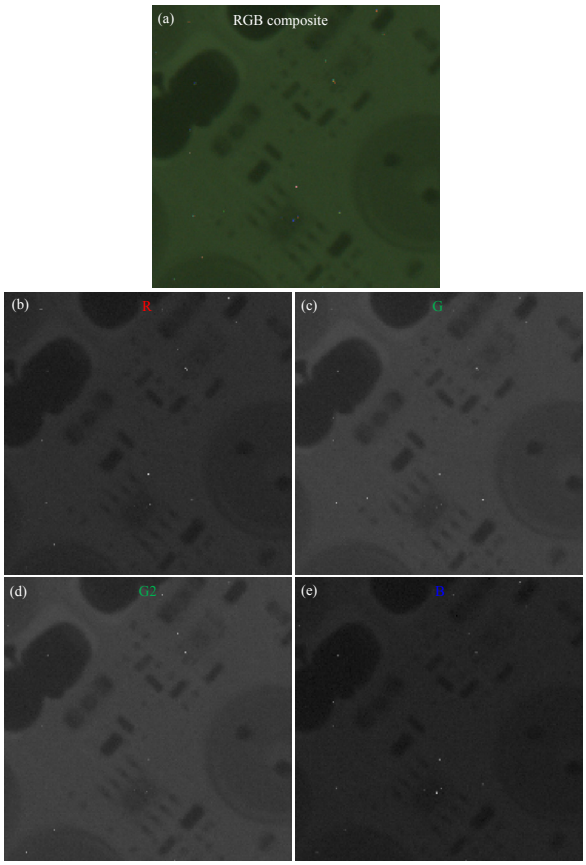

Fig. 3. Impulsive noise in the acquired RGB image and its raw images: (b)-(e) are the raw images for red, green, green, and blue before demosaicing to generate full-color image (a). Note that for a CR2 raw file, the output from the color filter array has the pattern RGGB.

impulsive noise here is random for each acquisition.

When analyzing the acquired image in Fig. 4(a) in the *HSV* color space shown in Figs. 4(b)-(d), we realized that different noisy pixels in a color image have different contributions from the corresponding pixels in the image from each *H*, *S*, and *V* channel. Note that modeling in *HSV* in our case is from the fact that the acquisition process takes an image from a scintillating screen. For the full information, we configured the camera to take a color image. The *HSV* color space is selected since an *HSV* representation models how colors appear under light, and the *HSV* model has a better color description for human interpretation.

Furthermore, the region contaminated by impulsive noise varies in each channel, as seen in Figs. 4(b)-(d). The size of the region also changes in each channel (the noise patch gets larger in the *H* channel, and smaller in *S* and *V* channels). This fact is found not only in the illustrated samples in Fig. 4, but also in all images acquired using our proposed imaging system (such as the one of a chest region in Fig. 5).

Based on this observation, we performed denoising on each channel (*H*, *S*, and *V*) separately. Since each channel was closed to noise that occurs in standard digital radiography, we employed a statistical-based impulsive noise filter [6] that was designed for standard digital

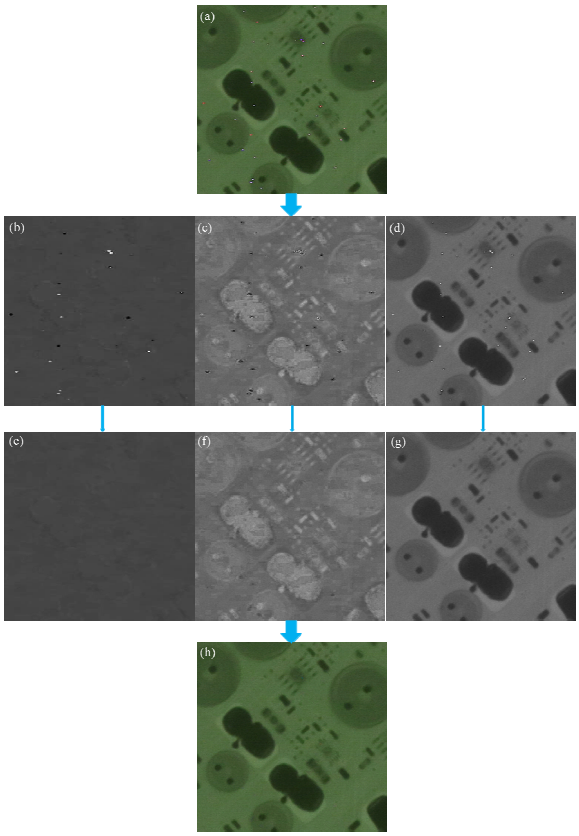

Fig. 4. Illustration of denoising an electronic circuit board image: (a) the noisy image; (b)-(d) *H*, *S*, *V* channels, respectively, of the noisy image; (e)-(g) *H*, *S*, *V* channels, respectively, of the denoised image; (h) the denoised image.

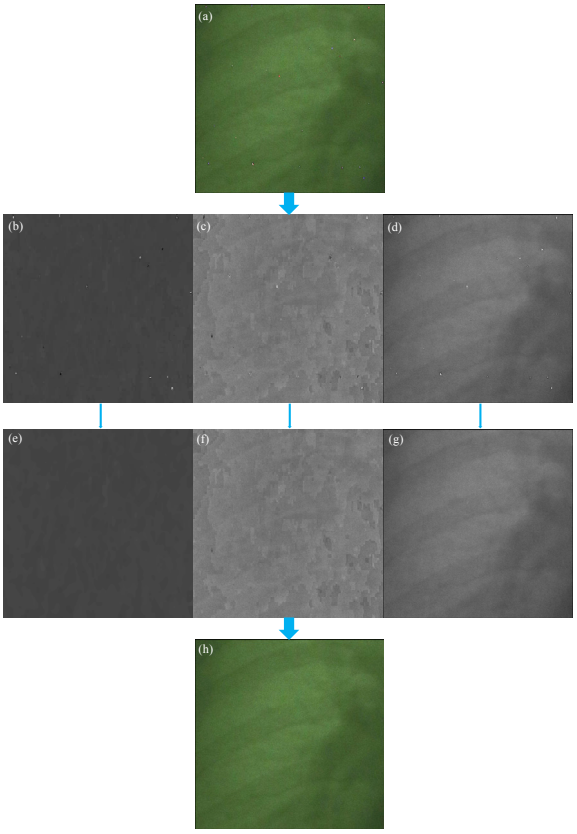

Fig. 5. Illustration of denoising a chest region: (a) the noisy image; (b)-(d) *H*, *S*, *V* channels, respectively, of the noisy image; (e)-(g) *H*, *S*, *V* channels, respectively, of the denoised image; (h) the denoised image.

radiography. (Note that in the image from our imaging system, the noise is not salt-and-pepper noise, since the region of degradation might occupy multiple pixels, and therefore, the standard salt-and-pepper noise filter cannot be used.)

The statistical-based impulsive noise filter [6] is based on a switching scheme where all pulses are first detected by a pulse detector. The detector assumes that the major contribution to image noise is made by the photon-counting process, with some pixels corrupted by impulsive noise. This assumption is generally true when acquiring an image in a controlled environment, as in our imaging system. Having the estimated pulses, the noisy image is filtered with a standard median filter.

In the images acquired by our proposed system, the area of pulses in the image of the H channel is usually larger than in the S and V channels. Therefore, depending on the conditions of X-ray acquisition, we need to apply the statistical-based impulsive noise filter more than one time to the image of the H channel, rather than just one time in the images of the S and V channels.

It is important to note that the median filter (and its median root prior in a Bayesian framework [11]) is very popular in radiographic imaging, since it does not alter the valuable information in the image. This is different from data-driven, state-of-the-art Gaussian or Poisson denoising methods, which tend to remove noise and promote non-realistic details in radiographic imaging.

Finally, note that in practice, since the radiologist has no difficulties detecting a signal in the presence of Poisson noise, we did not try to eliminate Poisson noise. Here, we aim to get rid of the unwanted impulsive noise that leads to a poor visualization result.

2.3 Model-based Image Deblurring

Unlike consumer imaging where there are many uncertainties during image acquisition, especially camera motion and object motion, the acquisition in digital radiography is performed in a controlled environment. Therefore, to quantify radiographic blur, researchers in the field usually use a parametric mathematical model to describe the blurring process. The general blurring processes are usually modeled as

$$y = x * k + n \tag{1}$$

where y is the observed blurry image, x is the latent sharp image, k is the approximated blur kernel, and n models noise.

In our particular X-ray imaging system, we denote $p_i^{(s)}$ as the PSF of the X-ray source blur on the detector plane at a source-to-object distance (SOD) of SOD_i and an object-to-detector distance (ODD) of ODD_i, where $p^{(d)}$ is the

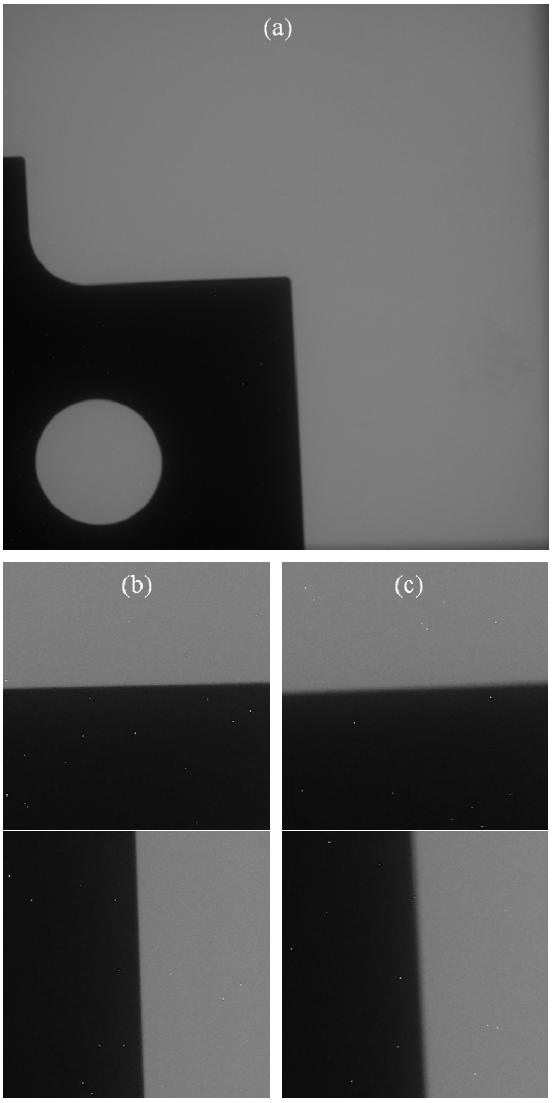

Fig. 6. (a) Image of the metal plate used to estimate the blur kernel; (b) extracted samples from an image when the distance from the object to the detector = 5 cm; (c) extracted samples from an image when the distance from the object to the detector = 40 cm.

PSF of the detector. Different from source blur, detector blur does not vary with SOD and ODD. We simplified the model by ignoring motion blur on the assumption the patient does not move during data acquisition. Then, the blurring process is modeled as follows:

$$y^i = x^i * k^i + n \tag{2}$$

where

$$k^i = p_i^{(s)} * p^{(d)} \tag{3}$$

is the blur kernel on the imaging plane, y^i is the observed blurry image, and x^i is the latent sharp image at SOD_i and ODD_i.

The PSFs ($p_i^{(s)}$ and $p^{(d)}$) are usually derived using data-driven approaches where it estimates PSF directly from radiographs of known objects [12, 13]. And in this work, we used a recently proposed systems approach to blur estimation and reduction (SABER) [12] for modeling and reducing the blur in our proposed X-ray DR imaging system. SABER consists of two steps: (i) estimation of the blur kernel; and (ii) deblurring using the estimated blur kernel.

To estimate the blur kernel, we illuminated a metal plate so it was perpendicular to the direction of the X-rays, and its edge was nearly horizontal and vertical. We acquire data when the object is placed in two different positions. In our experiment, one position was 5 cm from the detector (the scintillation screen) and the other was 40 cm (see Fig. 6). Having the two datasets, each with two projection images, the estimation involves the use of the L-BFGS-B algorithm (Details on blur kernel estimation can be found in [12]). Having the blur kernel, we can use either a Wiener filter [14] or a regularized least squares deconvolution (RLSD) algorithm to find sharp image x^i in (2). However, since the DR image has a huge size (with a resolution of about 4000×6000), we use a fast high-quality nonblind deconvolution based on adaptive-prior regularization [15], since it can find a state-of-the-art and stable deconvolution result in a relatively short time.

3. Results

To validate the performance of the proposed imaging system, as well as the denoising and deblurring methods, we acquired images from two objects: a human hand and an electronic circuit board. These samples were acquired by setting the following parameters in the scanner: accelerating voltage was 60 kV, the tube current was 160 mA, the distance from source to detector was 120 cm, and the distance from the scanning object to the detector was 2 cm.

Fig. 7 shows the acquired images with severe impulsive noise and the denoising results (using the standard median filter and the statistical-based impulsive noise filter). Using the statistical-based impulsive noise filter, almost all impulses were found, and the associated noise eliminated. Since the other image pixels remain untouched, the denoised image does not have any degradation (in comparison with the acquired noisy image). Meanwhile, the ordinary median filter could not reduce noise and preserve the radiographic features within the same time; the detail degraded while the noise remained, as indicated by the arrows at the top of Fig. 7(c). We conducted an independent image quality assessment with a radiologist, and the result confirmed the effectiveness of the proposed method in removing noise while retaining the radiographic information in the human hand. Note that the degree of noise in the acquired image is inversely proportional to the X-ray dose level passing through the patient—the lower the dose, the higher the noise. Therefore, our method to reduce noise is more important when reducing the X-ray dose.

Fig. 8 shows the results for the image of the electronic circuit board. Fig. 8(b) shows that in the denoised image,

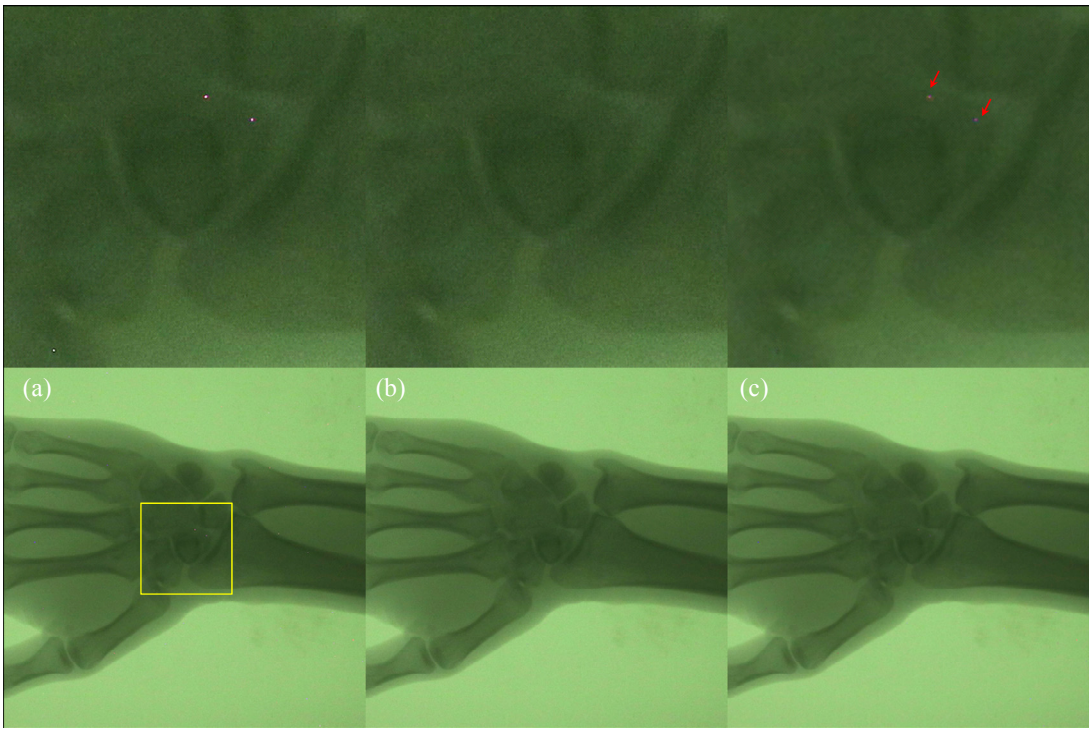

Fig. 7. Denoising result for a human hand: (a) the noisy image; (b) the image denoised by our method; (c) the image denoised by a median filter. Images on top of parts (a) to (c) are zoomed-in regions.

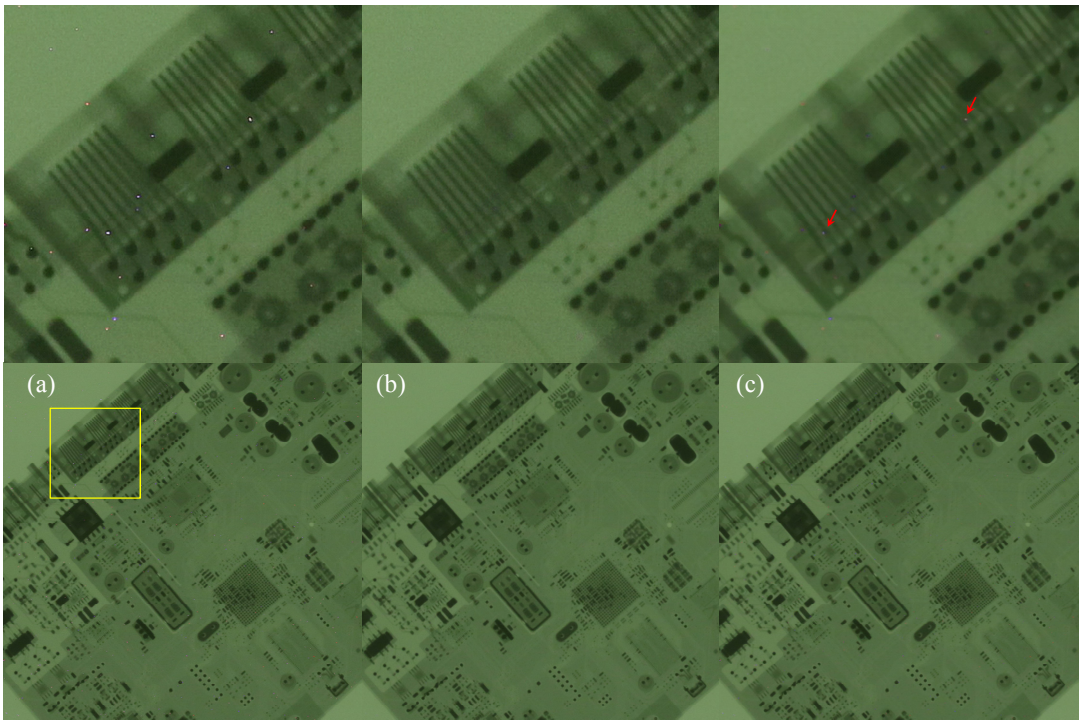

Fig. 8. Denoising results for an electronic circuit board: (a) the noisy image; (b) the image denoised by our method; (c) the image denoised by a median filter. Images on top of parts (a) to (c) are zoomed-in regions.

there was no loss of detail. Meanwhile, the standard median filter suffered loss of detail in the denoised images, as indicated by the arrows at the top of Fig. 8(c).

To check the effectiveness of the proposed method in eliminating noise while retaining radiographic detail, we show the results from chest-region imaging where the proposed method effectively removed impulsive noise while keeping most of the detail. See Fig. 9(b). The median filter removed the noise at the cost of degraded detail, as seen in Figs. 9(c) and (d). By using our method, the chest detail is preserved, as seen in Fig. 9(b), while it was degraded in Figs. 9(c) and (d). Note also that, by

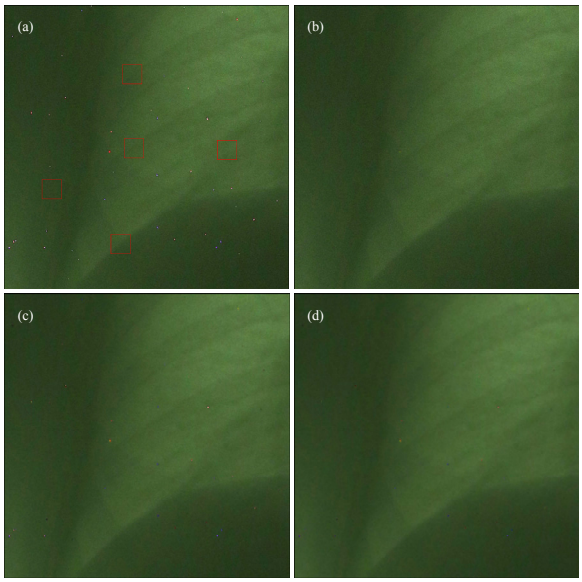

Fig. 9. Image denoising results for the chest region: (a) the noisy image; (b) the image denoised by our method; (c) images denoised by a median filter with a window size of 5×5; (d) images denoised by a median filter with a window size of 7×7. The highlighted red boxes in Fig. 9(a) indicate the ROI in order to calculate the error between the denoised images and the original noisy image.

Table 1. Percentage error measured on the denoised images.

ROI	Proposed method	Median filter with window size 5×5	Median filter with window size 7×7
1	**0.44**	2.52	3.03
2	**0.45**	2.56	3.02
3	**0.26**	2.26	2.68
4	**0.27**	2.34	2.83
5	**0.35**	2.42	2.86

increasing the window size in the median filter, the noise might be controlled in Fig. 9(d), but the detail is smoothed out.

To quantitatively evaluate the performance of the denoising approach, we selected regions of interest (ROIs) containing detail but no impulsive noise, as indicated in Fig. 9(a), and we then computed the percentage error (PE) between the denoised image and the noisy image. (The ROI without impulsive noise in the noisy image is considered ground truth, since it contains most of the information required by a radiologist.) The PE is given by:

$$\mathrm{PE} = \frac{\|x - \hat{x}\|}{\|x\|} \times 100\%,$$

where x is the noisy image, $\hat{x}$ is the denoised image, and $\|\cdot\|$ denotes the L_2 norm.

Table 1 lists the percentage error, showing that the proposed method achieved the smallest error with all

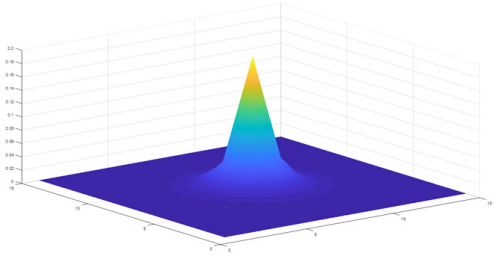

Fig. 10. Estimated blur kernel at a distance of 2 cm from the scintillating screen.

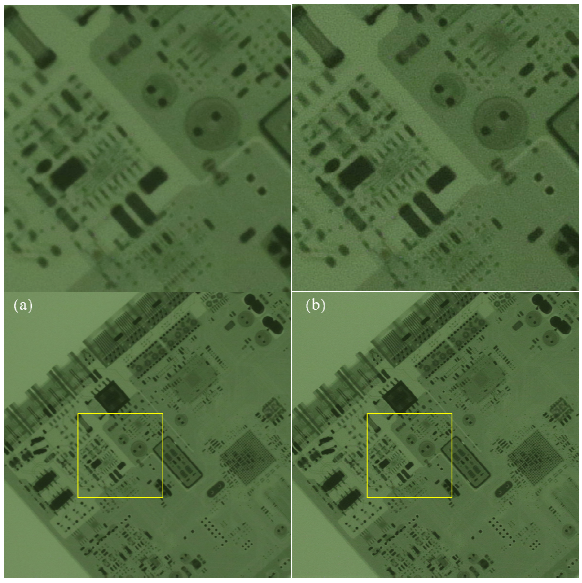

Fig. 11. Deblurring results for (a) the acquired image; (b) the deblurred image. Images in the top row are zoomed-in regions of the images in the bottom row. The global contrast factor for the acquired image is 1.52, while the value for the deblurred image is 1.73.

designated ROIs.

The problem in our case is significantly different from standard image denoising, where the image might be altered to eliminate noise. Therefore, we compared only the standard median filter against our method. (The other well-known impulsive image denoising methods tend to smooth out the detail and the shadow detail in the radiographic image.)

Regarding deblurring, the estimated blur kernel was found, and the one for the image plane at the distance of 2 cm from the detector is shown in Fig. 10. (Note that the final blur kernel was computed from two PSFs: source and detector.) That blur kernel was then used to deblur the acquired image, and the deblurred result is shown in Fig. 11. To evaluate the quality of the deblurring method, we measured the global contrast factor (GCF) [16] for the original and deblurred images. GCF is considered a global focus measure, and is strongly correlated to human assessment in terms of the degree of focus of the image, where the higher the value, the better the degree of focus. The measured GCF value for the original image was 1.52, and the one for the deblurred image was 1.73. (The results for the zoomed-in region were 2.47 for the original image

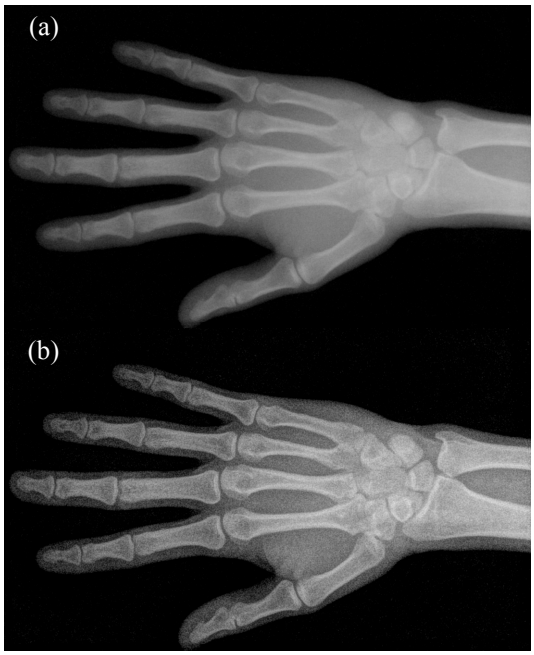

Fig. 12. (a) The acquired image (in grayscale); (b) the post-processed image.

and 2.71 for the deblurred image).

As shown in Fig. 11(b), the deblurred image has sharper edges and is richer in detail. More importantly, it does not generate an artificial pattern in the deblurred image (as with the standard image-sharpening algorithm) since the PSF was systematically acquired. Since the deconvolution algorithm is a regularization method, we can control the degree of smoothness in the deblurred image with a special hyperparameter. The image in Fig. 11 was restored with a manually, specifically selected value of that hyperparameter.

Finally, to show the overall performance of the proposed imaging system in radiography, Fig. 12 is a final image that went through the image processing pipeline. Compared to the acquired image, the radiological features were preserved and are clearly displayed. In this particular case, the bone contrast was adjusted to satisfy the requirements of the radiologist.

4. Conclusion

In this paper, we proposed and tested an imaging system to acquire digital radiography images using a consumer camera. To improve the image quality, we used a statistical-based impulsive noise removal method to get rid of impulsive noise where the rate is low but it significantly degrades the visualization results. We also used parametric modeled non-blind deconvolution to deblur the image.

Experiments show that the denoising method is capable of efficiently eliminating impulsive noise while preserving detail in the digital radiography images. Meanwhile, for deblurring, by combining a systems approach to blur estimation with fast non-blind deconvolution, we can accurately and quickly recover a sharp image from a blurred image.

The proposed imaging system, and denoising and deblurring methods, when plugged into an image processing pipeline, can quickly provide DR images with fine detail, and can be useful for radiography.

Though we tested our imaging system with only one particular type of camera, our denoising and deblurring methods are expected to work well with other cameras. An investigation on the use of other cameras in our imaging system is beyond the scope of this paper. However, we expect using our imaging system with different cameras will work well, since similar studies have been conducted in the field [4, 17].

References

[1] E. Seeram, *Digital Radiography - Physical Principles and Quality Control*. Springer, 2019. Article (CrossRef Link)

[2] J.T. Bushberg, J.A. Seibert, E.M. Leidholdt Jr, J.M. Boone. *The essential physics of medical imaging*. 3rd ed. Philadelphia, PA: Lippincott Williams & Wilkins; 2012. Article (CrossRef Link)

[3] A. Panna, A.A. Gomella, K.J. Harmon, P. Chen, H. Miao, E.E. Bennettand H. Wen, "Performance of low-cost X-ray area detectors with consumer digital cameras," *Journal of Instrumentation*, Vol. 10, No. 05, pp. T05005, May 2015. Article (CrossRef Link)

[4] H.X. Fan. *Lens-coupled X-ray imaging systems*. PhD Dissertation, University of Arizona, 2015. Article (CrossRef Link)

[5] K. Umetani, Y. Kawata and N. Niki, "Development of 36M-pixel x-ray detector for large field of view and high-resolution micro-CT," *Proceedings of SPIE*, pp. 1002005, October 2016. Article (CrossRef Link)

[6] I. Frosio and N. A. Borghese, "Statistical based impulsive noise removal in digital radiography", *IEEE Transactions on Medical Imaging*, Vol. 28, No. 1, pp. 3-16, January 2009. Article (CrossRef Link)

[7] V. Nieuwenhove, J. De Beenhouwer, F. De Carlo, L. Mancini, F. Marone. and J. Sijbers, "Dynamic intensity normalization using eigen flat fields in X-ray imaging". *Optics Express*, Vol. 23, No. 21, pp. 27975-27989, October 2015. Article (CrossRef Link)

[8] R.V. Metter and D. Foos, "Enhanced latitude for digital projection radiography", *SPIE 3658, Medical Imaging 1999: Image Display*, May 1999. Article (CrossRef Link)

[9] P. Irrera, I. Bloch, M. Delplanque, "A flexible patch based approach for combined denoising and contrast enhancement of digital X-ray images", *Medical Image Analysis*, Vol. 28, pp. 33-45, February 2016. Article (CrossRef Link)

[10] S. Dippel, M. Stahl, R. Wiemker, and T. Blaffert, "Multiscale contrast enhancement for radiographies: Laplacian pyramid versus fast wavelet transform", *IEEE Transactions on Medical Imaging*, Vol. 21, No. 4, pp. 343-353, April 2002. Article (CrossRef Link)

[11] S. Alenius and U. Ruotsalainen, "Generalization of median root prior reconstruction", *IEEE Transactions*

on Medical Imaging, Vol. 21, No. 1, pp. 1413 - 1420, November 2002. Article (CrossRef Link)
[12] K. Aditya Mohan , R. M. Panas , and J. A. Cuadra, "SABER: A Systems Approach to Blur Estimation and Reduction in X-ray Imaging," *IEEE Transactions on Image Processing*, Vol. 29, pp. 7751-7764, July 2020. Article (CrossRef Link)
[13] P. Russo and G. Mettivier, "Method for measuring the focal spot size of an X-ray tube using a coded aperture mask and a digital detector", *Medical Physics*, Vol. 38, No. 4, pp. 2099-2115, March 2011. Article (CrossRef Link)
[14] F. Orieux, J.-F. Giovannelli, and T. Rodet, "Bayesian estimation of regularization and point spread function parameters for Wiener-Hunt deconvolution", *Journal of the Optical Society of America. A Optics, Image Science, And Vision*, Vol. 27, No. 7, pp. 1593- 1607, July 2010. Article (CrossRef Link)
[15] H.E. Fortunato and M.M. Oliveira, "Fast high-quality non-blind deconvolution using sparse adaptive priors", *The Visual Computer*, Vol. 30, pp. 661-671, May 2014. Article (CrossRef Link)
[16] K. Matković, L. Neumann, A. Neumann, T. Psik and W. Purgathofer, "Global contrast factor - a new approach to image contrast", *Proceedings of the First Eurographics conference on Computational Aesthetics in Graphics, Visualization and Imaging*, pp. 159-167, May 2005. Article (CrossRef Link)
[17] A. Panna *et al*, "Performance of low-cost X-ray area detectors with consumer digital cameras", *IOP Journal of Instrumentation*, Vol. 10, pp. T05005, May 2015. Article (CrossRef Link)

Van-Giang Nguyen received the B.S. degree in computer science from Le Quy Don Technical University, Hanoi, Vietnam, in 2005, and the M.S. and Ph.D. degrees in electronic engineering from Paichai University, Daejeon, Korea, in 2009 and 2012, respectively. Since 2013, he has been with the Department of Information Systems, Le Quy Don Technical University, Hanoi, Vietnam. His current research interests include image processing, computer vision, and their applications to medical imaging and medical physics.